ACS APPLIED MATERIALS & INTERFACES

RESEARCH ARTICLE

www.acsami.org

Deposition of Amorphous CN_x Materials in BrCN Plasmas: Exploring Adhesion Behavior as an Indicator of Film Properties

Joshua M. Stillahn, Kristina J. Trevino, and Ellen R. Fisher*

Department of Chemistry, Colorado State University, Fort Collins, Colorado 80523-1872, United States

ABSTRACT: Adhesion and delamination behavior of amorphous carbon nitride (a-CN_x) is critical to development of wear resistant materials and protective coatings. Here, the composition and delamination behavior of a-CN_x films was explored utilizing BrCN, CH_3CN, and CH_4 as film precursors, either alone or in combination with one another. Film delamination depends on film thickness and plasma composition as well as post deposition treatment conditions. Delamination is not observed with films deposited from 100% CH_3CN discharges, whereas films of similar thickness deposited from 100% BrCN plasmas delaminate almost immediately upon exposure to atmosphere. Exploration of these differences in delamination behavior is discussed relative to contributions of humidity, hydrocarbon species, and ion bombardment during deposition in conjunction with compositional studies using X-ray photoelectron spectroscopy (XPS).

KEYWORDS: plasma, chemical vapor deposition, coatings, xps

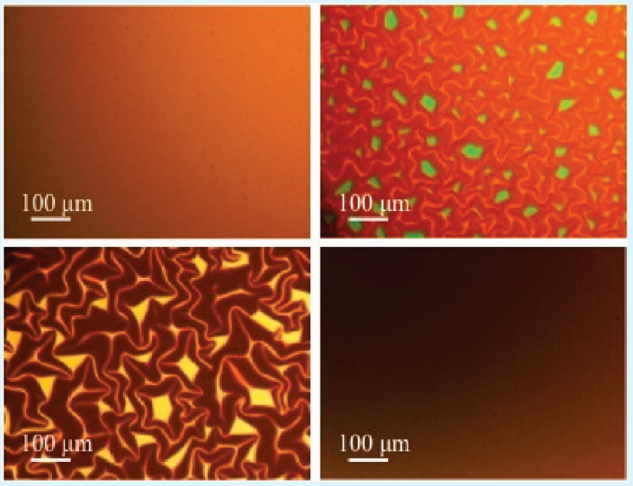

INTRODUCTION

Advanced materials systems, such as ultralarge scale integrated circuits, various protective coatings, solar cells, and magnetic memory devices rely on multilayer devices integrating different types of materials. As such, a key factor in the efficacy of these systems and devices is the robustness of film/substrate and film/film interfaces, specifically with respect to mechanical properties.[1−3] In particular, films that undergo thermal changes, radiation exposure, or ion bombardment can deform, crack, or delaminate from the underlying substrate causing device failure. In addition, diffusion of reactive species such as water or ions can also result in delamination or cracking.[3−5] In many instances, protective coatings as well as dielectric materials in integrated circuits are formed using plasma-enhanced chemical vapor deposition (PECVD), a method that has numerous advantages, but which also often exposes the film to a range of high energy species that can ultimately contribute to mechanical failure of the resulting material. Thus, examination of the mechanical performance and reliability of film/substrate interfaces created via PECVD is an important component of understanding the entire plasma deposition process.

Studies of amorphous carbon nitride (a-CN_x) deposition in PECVD systems often focus on precursor mixtures, such as CH_4/N_2, which allow independent control over C and N densities in the gas phase. Previous results from our lab highlight the relatively high surface reactivity of CN radicals in CH_4/N_2 discharges,[6] but the chemical complexity of these mixed systems limits the confidence with which one can establish the contribution of CN radicals to the deposition process. In an effort to alleviate some of this ambiguity, this work was extended to include the study of CN in CH_3CN discharges, effectively using a single source precursor rather than a mixed gas system.[7] Similarly high surface reactivities were observed, and accompanying deposition studies suggest that these surface reactions favor the incorporation of CN during film deposition. In a similar vein, we also explored the use of BrCN as an alternative precursor system for CN generation; results from those studies[8] were used to develop our molecular-level understanding of the relationship between the internal energy of a specific plasma species (CN) and its surface reactivity.

For several reasons, the BrCN system presents an interesting opportunity for further expansion of these studies. Aside from the substantially elevated CN rotational temperatures we measured in BrCN plasmas,[8] literature studies suggest that BrCN may generate some rarely observed quartet electronic states of CN,[9,10] which could, in turn, affect their incorporation into a-CN_x films.[11] BrCN is also well-suited to the reductionist approach we have taken to studying a-CN_x systems as it allows observation of CN radical behavior in the absence of other depositing species, such as H or CH_x species. Because CN is the primary deposition species in BrCN discharges, it becomes feasible to deposit a-CN_x materials that do not contain hydrogen. Such films have been shown to exhibit substantially different microstructures and mechanical properties,[12−15] thereby creating a possible link

Received: December 29, 2010
Accepted: March 18, 2011
Published: March 21, 2011

between the molecular level plasma chemistry and possible performance and reliability issues with a-CN_x films. Notably, films without hydrogen are predominately obtained by sputtering graphite in a N_2 atmosphere, and reports of the formation of H-free a-CN_x by PECVD are few.[15,16]

Here, we present results from our investigation of a-CN_x deposition in plasma systems containing BrCN. In addition to complete characterization of film composition using Fourier transform infrared spectroscopy (FTIR) and X-ray photoelectron spectroscopy (XPS), we also compare the optical and mechanical properties of films deposited from BrCN and CH_3CN plasmas as well as films deposited using systems containing additional hydrocarbons. As anticipated, the adhesion behavior of the a-CN_x films is a critical aspect of the reliability of these materials. Given the challenges of using such materials in commercial applications, our work has focused on evaluating the respective contributions of three factors to explain the observed film adhesion behavior, namely humidity, ion bombardment, and Br content in the film.

EXPERIMENTAL DETAILS

The experimental apparatus used for film deposition has been described in detail previously.[17] The reactor consists of two glass tubes (50 mm i.d.) joined by an O-ring (58 mm i.d., 3.5 mm cross-section) to allow access to the interior of the reactor. The main barrel of the reactor is ~48 cm long. Feed gases enter the reactor through a 6 mm i.d. inlet stem and unreacted gases are pumped away by a two-stage rotary vane mechanical pump (2 L/s). As described previously,[7] the substrate stage and substrate temperature can be monitored with a K-type thermocouple connected to the stage. Glass sleeves (43 mm i.d.) were inserted in the main barrel of the reactor to allow exchange of heavily deposited surfaces, and the reactor and sample stage were cleaned by an oxygen plasma prior to each deposition. Substrates (20 × 20 mm p-type Si (100) with native oxide) were placed on the substrate stage prior to deposition. The pressure in the chamber was monitored with an MKS Baratron capacitance manometer and was allowed to stabilize before initiating the discharge. For a-CN_x depositions, plasmas containing either a single precursor (BrCN or CH_3CN) or mixtures of BrCN (Sigma Aldrich, 97%), CH_3CN (Fisher Scientific, 99.8%), and CH_4 (Airgas, 99.9%) were used. Both CH_3CN and BrCN precursors were subjected to a minimum of three freeze−pump−thaw cycles prior to use to remove trapped atmospheric gases. For all depositions, the pressure was maintained at 100 ± 2 mTorr and the applied rf power was maintained at 50 ± 2 W. Deposition times ranged from 10 to 40 min. Following deposition, the plasma discharge was stopped, and the flow of precursor was continued for 20 min to minimize the effect of oxidation upon exposure to atmosphere as this technique has been shown to help quench free radicals formed in the plasma polymerization process.[18]

Surface Topography and Morphology. Surface morphology and topography were characterized with scanning electron microscopy (SEM) and cross-sectional SEM, using a JEOL JSM 6500F field emission microscope with an accelerating voltage of 15 keV. To prevent charge buildup on the substrate surface during analysis, ~1 nm of Au was sputtered onto the surface by an Anatech sputter coater prior to imaging. For top-down analysis, the substrates were affixed to a standard SEM stub by double-sided Cu tape (3 M brand). Surface images were also obtained using a commercial Nikon phase contrast microscope.

Film Composition. Film composition was explored using FTIR and XPS. FTIR spectra were obtained using a Nicolet Magna 760 spectrophotometer, with a resolution of 8 cm^{-1} and averaging over 65 scans. The spectra shown were only corrected for a sloping baseline. XPS analyses were performed on deposited films using a PHI-5800 ESCA/AES spectrometer. A monochromatic Al Kα X-ray source (1486.6 eV) at 350 W and 15 kV was used for all data sets. Spectra were collected with a photoelectron takeoff angle of 45°. Survey scans were collected with a pass energy of 93.90 eV and high-resolution spectra were acquired with a pass energy of 23.50 eV. Charge compensation was accomplished with an electron flood gun with a 16 eV accelerating voltage. Elemental analysis and smoothing were performed using Matlab based software, Multipak; peak deconvolution was performed using XPS Peak 4.1 software. All samples were sputtered with ~1 nm of Au to prevent charge buildup on the surface. Shifts in the C_{1s} peak positions were determined by shifting the Au peak to 85.0 eV. All peaks were assumed to be 100% Gaussian and the fwhm was limited to 2.5 eV unless otherwise indicated.

Film Thickness and Optical Properties. The thicknesses of films deposited were measured by variable angle spectroscopic ellipsometry (VASE) using a Woollam M-2000 model DI ellipsometer over a spectral window of 300−1100 nm with incident angles of 55, 65, and 75°. The resulting spectroscopic data were modeled using WVASE software provided by the instrument manufacturer to extract information about the film thickness and optical properties.

Determination of a-CN_x film thickness from VASE data was performed by optimizing the fit between the experimental and simulated ellipsometric data. The general model used to describe the film cross-section is made up of four regions. The first region is a 1 mm thick layer of Si with optical constants corresponding to those reported by Jellison.[19,20] Above this, a semiconducting layer was included to model the thin layers of disordered Si that may exist on the surface of a Si substrate; the thickness of this layer varied from 0 to 15 nm. The third region of the general model corresponds to the deposited a-CN_x film and was modeled with one or more layers, each described using the Cauchy dispersion model, which is commonly used to model ellipsometric data for amorphous materials. For multilayer films, multiple Cauchy layers were included in the model to optimize the fit. In addition, the thickness of the individual layers describing the a-CN_x films varied depending on growth rate and deposition time. The final component of the general model describes the roughness of the film sample and consists of an effective medium approximation (EMA) layer composed of a 50/50 mixture of the underlying Cauchy layer and voids (air).

Our optical transmission and absorption data indicate that the a-CN_x films generally exhibit a strong absorption at $\lambda < 450$ nm. At these wavelengths, the reliability of the Cauchy model is limited; thus, the ellipsometric data were initially fit over the range of wavelengths where the material is highly transparent. Using these data, the optical constants for n and k were then fit in a point-by-point manner over the remaining wavelengths to encompass all of the experimental data. The above process consistently produced reasonably good fits with mean standard errors (MSE) ≤ 10.

The optical band gaps, E_g, of the a-CN_x films were determined through additional analysis of the ellipsometric data. Using the data analysis software, the Cauchy layer describing the a-CN_x film was used as a reference material in a Tauc−Lorentz oscillator layer. The Tauc−Lorentz model describes a material as a collection of absorption peaks, or oscillators, and is better-suited for extracting information from ellipsometric data over wavelengths where the material absorbs. The generated Tauc−Lorentz data were fit to the experimental data, and k values were used to obtain optical absorption coefficients, α, at each wavelength according to the dispersion relation of k

$$\alpha = \frac{4\pi k}{\lambda} \quad (1)$$

The Tauc band gap, E_{Tauc}, is then determined from the Tauc relation, eq 2

$$E\alpha(E) = A(E - E_{Tauc}) \quad (2)$$

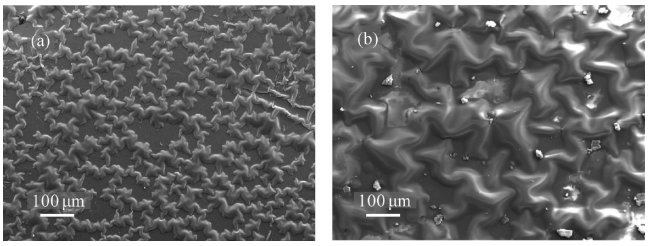

Figure 1. SEM micrograph of CN_x film on a KBr pellet after exposure to atmosphere. The films were prepared in 100% BrCN plasma (100 mTorr, 50 W) with deposition times of (a) 20 min and (b) 60 min. Magnification for both images is 130×.

by extrapolating the linear portion of a plot of $(\alpha E)^{1/2}$ as a function of E to find the x-intercept. In cases where the Tauc plot did not exhibit a clear region of linearity, the slope was determined from a linear fit to several points near where $(\alpha E)^{1/2}$ starts to increase. The reproducibility of this method for quantifying E_{Tauc} is reflected in the relatively small standard deviations obtained from our data.

RESULTS AND DISCUSSION

A range of plasma gas mixtures were used to explore the effects of deposition parameters on the resulting a-CN_x film properties, most notably adhesion/delamination and film composition. Our observations of films deposited in 100% BrCN discharges indicate that when the films are exposed to atmosphere following deposition, they tend to delaminate from the underlying substrate and become visibly rougher. SEM provides a more detailed picture of the film morphology and evidence for delamination upon exposure to atmosphere. Figure 1 contains micrographs for films deposited in a 100% BrCN plasma (100 mTorr, 50 W), clearly showing that the films have buckled into ridgelike structures. The time required for delamination decreases at longer deposition times (i.e., for thicker films), and, as comparison of Figure 1a,b shows, ridges formed at longer deposition times are substantially larger.

Similar delamination behavior has been reported by other researchers in the deposition of carbon nitride[21] and boron nitride materials.[4] These studies highlight the role of humidity and material stresses in delamination. Peponas et al. employed infrared absorption spectroscopy measurements to hypothesize that delamination involves chemical reactions between H_2O and isocyanate (R−C═N═O) groups at the film−substrate interface.[22] Although this type of absorption spectroscopy constitutes a bulk characterization technique and thus does not provide conclusive evidence of interfacial reactions, the data show that the process of delamination is not simply a mechanical phenomenon, but involves chemical changes as well.

Another notable aspect of both the boron nitride and carbon nitride studies is that they involve materials deposited by sputter coating; our observation of the same delamination behavior in PECVD systems suggests there are some basic chemical similarities between films deposited with the two deposition methods. Interestingly, however, we do not observe delamination of films deposited in 100% CH_3CN plasmas. This is illustrated by the phase contrast microscope images shown in Figure 2. Contrast in these images arises from interference following optical phase retardation as light interacts with different parts of the sample, and the puckering or ridges formed by the delaminated film become very apparent. The film deposited in a 100% CH_3CN plasma does not delaminate and has a uniform appearance throughout the field of view, Figure 2a, whereas the film deposited in a 100% BrCN plasma very clearly has delaminated from the substrate, Figure 2b. Benlahsen and co-workers characterized the cross sections of delamination ridges like those shown in Figure 2 to extract information on the mechanical stress in the material.[21] This is discussed further below.

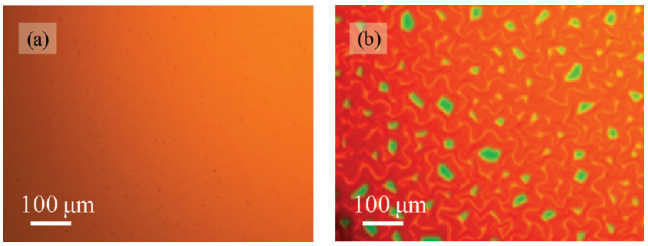

Figure 2. Phase contrast microscope images of films deposited for 40 min in (a) 100% CH_3CN and (b) 100% BrCN plasmas. In each case, total gas pressure = 100 mTorr and rf power = 50 W.

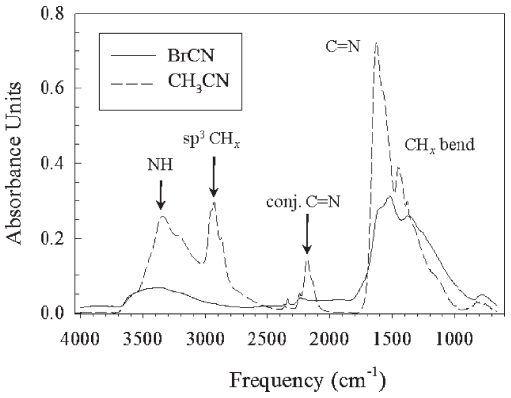

Figure 3. Corrected transmission FTIR spectra of film deposited for one hour on a KBr substrate in 100% BrCN (solid line) and 100% CH_3CN (dashed line) plasmas.

Chemical characterization of the films produced in our plasmas was pursued with FTIR absorption spectroscopy and XPS. The FTIR spectra for films deposited on KBr pellets in 100% CH_3CN and 100% BrCN plasmas are shown in Figure 3. The absorption features in the region of 1500 cm^{-1} are assigned to C═N stretching and CH_x bending modes, and similar features are apparent for the films deposited in 100% BrCN plasmas. Similarly, the broad absorption centered near 3400 cm^{-1} is visible in both spectra, though more well-defined absorption bands somewhat obscure this feature in the spectrum of the film deposited from a 100% CH_3CN plasma. We assign this broad absorption band to C═NH, but it has been associated with OH stretching in the work of Benlahsen and co-workers.[22] Further studies are needed to resolve this discrepancy, but this absorption band may prove useful in understanding the effects of H_2O on delamination behavior. The absence of sharp NH and sp^3 CH_x stretching modes in the BrCN films is not surprising, as we do not expect to have hydrogen in the discharge. The lack of conjugated C═N absorption in the BrCN film is notable, however, as this is indicative of differences in the microstructure of the two films. It is also important to note that the absorption spectrum shown in Figure 3 for the film deposited in a BrCN plasma was measured after the films had buckled, and may not accurately portray the

composition and structure of the virgin material.[22] Subsequent investigation of film delamination focused on establishing fundamental connections between the behavior of films deposited in the different plasma systems. As the composition and morphology of pressed KBr pellets can be unpredictable, Si wafers were used as substrates for the remainder of the studies.

High-resolution C_{1s} XPS spectra for films deposited on Si substrates in 100% BrCN and 100% CH_3CN plasmas are shown in Figure 4. The C_{1s} spectrum for films deposited in 100% BrCN plasmas, Figure 4a, exhibits three major peaks at 285.0, 287.0, and 288.9 eV designated as C−C/C−H, C═N (sp^2 carbon), and C−N (sp^3 carbon), respectively. Although the same peaks appear in the spectrum for the film deposited in 100% CH_3CN, Figure 4b, their respective contributions to the total peak area differ dramatically. Specifically, films deposited in 100% BrCN plasmas have a larger fraction of sp^2 and sp^3 carbon, which has been identified as contributing to delamination in a-CN_x films.[5,23] Note that XPS elemental analysis, Table 1, reveals our films contain small amounts of oxygen; thus, the two peaks assigned to C═N and C−N could also contain C═O and C−O moieties as contributions from oxygen-containing species are not resolvable from those of nitrogen-containing species.

Films deposited from BrCN plasmas also contain small but significant levels of bromine, Table 1. Figure 5 contains the high resolution Br_{3d} XPS spectrum for a film deposited from 100% BrCN. There are four different binding environments, suggesting bromine is incorporated in these films in different forms. Notably, the largest peak at ~70.8 eV can be attributed to bromine covalently bonded to carbon.[24] The smaller peak at higher binding energies (72.2 eV) likely corresponds to oxybrominated derivatives (BrO_x^-) as these are the only species with higher binding energies than covalently bound bromine. The two peaks at 69.3 and 68.2 are assigned to bromide (Br^-) species, most likely in the form of physisorbed BrH, and C−Br_2 surface charge transfer complexes, respectively.[24] Given the relatively high contributions from bromine not covalently bound to carbon, we anticipate that heating or prolonged exposure to atmosphere could decrease or eliminate the bromine from these films.

One of the inherent conclusions in the work of Benlahsen and co-workers is that their materials were porous enough to allow the diffusion of water vapor to the film−substrate interface, and they suggest that this property arises because their films have a high density of terminating functional groups (e.g., C−N and C═N) in the film network.[21] The films we deposited in BrCN plasmas delaminated over a period of time that was dependent on both humidity and deposition time. Increases in either parameter shortened the time required for delamination, and for thick films (thickness >500 nm) that were quickly transferred to a humid

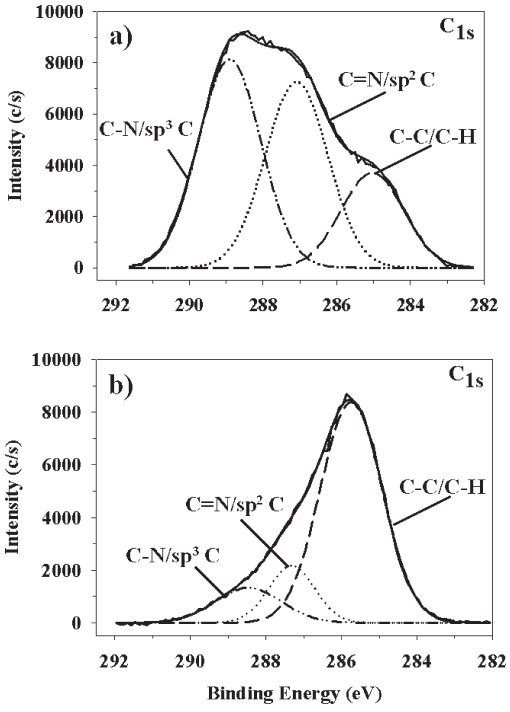

Figure 4. High-resolution C_{1s} XPS spectra for a film deposited in (a) 100% BrCN and (b) 100% CH_3CN plasmas. Both spectra are for freshly deposited samples and contain three binding environments: C−C/C−H (long dash), C═N, sp^2 carbon (dotted line), and C−N, sp^3 carbon (dash-dot-dot). Plasma conditions were: 100 mTorr and 50W for 40 min.

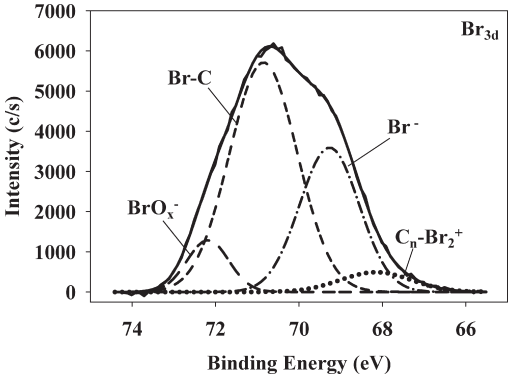

Figure 5. High-resolution Br_{3d} XPS spectrum for a film freshly deposited in a 100% BrCN plasma, containing four binding environments BrO_x^- (medium dash); Br covalently bonded to carbon (short dash); Br^- (dash-dot); and C_n-Br_2 (dotted). Plasma conditions were: 100 mTorr, 50 W for 40 min.

Table 1. XPS Percent Composition and C/N Ratios for Freshly Treated and Aged Samples

		%C	%N	%O	%Br	%Au	C/N
100% BrCN	fresh	42.0 ± 3.2	35.1 ± 4.0	12.5 ± 0.0	6.7 ± 1.3	3.7 ± 1.0	0.8 ± 0.2
	aged	55.8 ± 2.0	30.0 ± 1.9	8.0 ± 0.3		6.2 ± 0.4	0.5 ± 0.1
100% CH_3CN	fresh	64.4 ± 1.9	19.6 ± 1.3	9.2 ± 1.2		6.8 ± 2.0	0.3 ± 0.0
	aged	59.5 ± 1.1	21.0 ± 1.0	15.0 ± 2.2		4.5 ± 0.3	0.4 ± 0.0
50:50 BrCN/CH_4	fresh	61.2 ± 1.5	2.5 ± 1.1	9.2 ± 1.3		4.6 ± 1.0	0.4 ± 0.0
	aged	66.3 ± 3.3	11.3 ± 2.7	18.3 ± 0.2		4.1 ± 1.0	0.4 ± 0.1
100% BrCN:N_2 plasma-treated	fresh	39.1 ± 1.3	36.9 ± 1.5	13.5 ± 2.0	6.9 ± 1.6	3.7 ± 0.8	1.1 ± 0.1

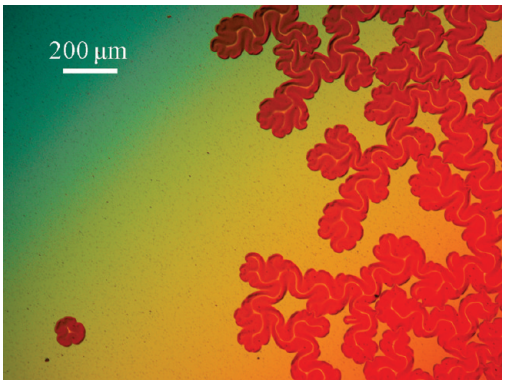

Figure 6. Phase contrast microscope image of CN_x film deposited on Si in a 100% BrCN plasma (100 mTorr, 50 W) for 40 min.

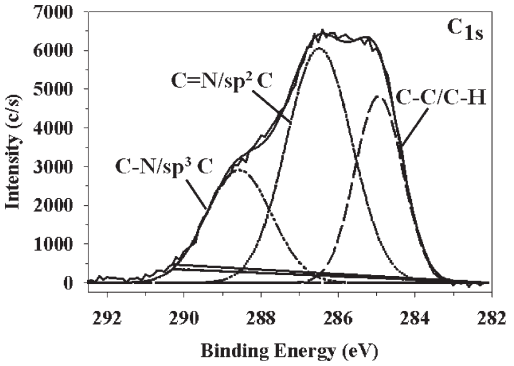

Figure 7. High-resolution C_{1s} XPS spectra for a film deposited in a 50:50 $BrCN/CH_4$ plasma. The spectrum is for a freshly deposited sample and contains three binding environments: C−C/C−H (long dash), C═N, sp^2 carbon (dotted line), and C−N, sp^3 carbon (dash-dot-dot). Plasma conditions were: 100 mTorr and 50W for 20 min.

environment, delamination took place immediately. In contrast, films deposited for shorter times and removed in the ambient laboratory environment took anywhere from 30 s to a few hours to delaminate. Additional behavior indicative of the diffusion of water through our materials[25,26] can be observed with phase contrast microscopy as in Figure 6. Here, a delamination "island" is observed in the lower-left corner of the image, indicating that the porous structure of the film allows delamination to proceed not only from the corners and edges of the substrate, but in isolated regions of the film as well.

One possible reason for why film adhesion differs so dramatically between BrCN and CH_3CN discharges is that the films deposited in BrCN plasmas are less cross-linked (i.e., have a higher density of terminating functional groups) than films deposited in CH_3CN discharges. To mirror the gas phase composition in CH_3CN discharges, CH_4 was added to the BrCN systems, thereby adding a purely hydrocarbon (i.e., CH_x) component to the flow. In addition to changes associated with the codeposition of CH_x and CN species in $BrCN/CH_4$ discharges, we anticipated that the presence of atomic H might also favor increased cross-linking during deposition. This idea is supported by mechanistic studies of diamond-like carbon (DLC) deposition by Von Keudell and co-workers[27] who found that atomic H can abstract terminating H atoms from the surface of a growing film to create active sites. The presence of these active

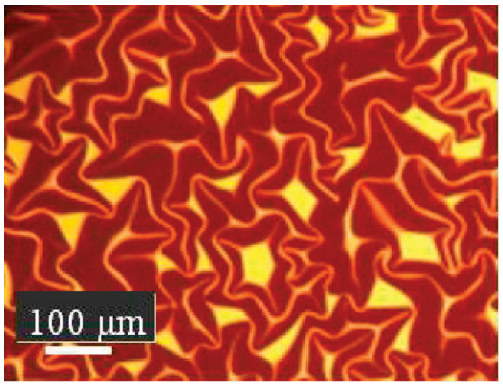

Figure 8. Phase contrast microscope image of a film deposited for 40 min in a 50:50 $BrCN/CH_4$ plasma. The total gas pressure = 100 mTorr and rf power = 50 W.

sites promotes cross-linking as additional precursors (particularly CH_3) arrive at the DLC film growth front. The observation of CH_x^+ and H* in CH_3CN plasmas[7] along with the abundance of unsaturated C≡N bonds would favor such a mechanism in a-CN_x deposition as well. Indeed, the same strategy was shown by Kim et al. to improve the adhesion of carbon-containing boron nitride (BN:C) materials obtained by PECVD, with reductions in both the compressive stress of the material and its susceptibility to humidity.[28]

A high-resolution C_{1s} XPS spectrum for a film deposited from a 50:50 $BrCN/CH_4$ plasma is shown in Figure 7. This spectrum has the same binding environments of that collected for the film deposited from 100% BrCN, Figure 4a. The primary difference is that the C−C/C-H peak in the film deposited from the $BrCN/CH_4$ plasma is significantly higher than the same peak in the film deposited from 100% BrCN. This suggests $BrCN/CH_4$ films would also be unstable with respect to delamination. Figure 8 contains an optical micrograph of a film deposited in a plasma containing equal partial pressures of BrCN and CH_4, clearly showing delamination has occurred. This indicates that even with additional hydrocarbon, the resulting film remains porous enough to allow diffusion of water vapor to the interface. Such images suggest that the presence of hydrocarbons and atomic H does not sufficiently alter the deposition chemistry so as to prevent film delamination.

Given that our a-CN_x films are susceptible to humidity, an additional factor to consider is possible effects of aging. Figure 9 shows XPS high-resolution C_{1s} spectra for aged films deposited in the three plasma systems: 100% BrCN, 100% CH_3CN, and 50:50 $BrCN/CH_4$. Comparison of C_{1s} spectra for aged and fresh samples reveals that aging dramatically changes the binding environment in the films. For the films deposited from plasmas containing BrCN, we see a sharp increase in the C−C/C−H peak, which is likely the result of adventitious carbon being incorporated during the aging period, Table 1. In contrast, the C_{1s} binding environments in the film deposited from CH_3CN have shifted from primarily C−C/C−H to sp^2 and sp^3 carbon bonded to nitrogen and/or oxygen. We also measure a concomitant increase in both nitrogen and oxygen content in these films, Table 1. Thus, these films appear to oxidize with time, whereas the films deposited from BrCN systems do not. Notably, the aged film deposited from the 100% BrCN plasma does not contain any Br, consistent with our analysis of the Br_{3d} spectrum for the fresh films.

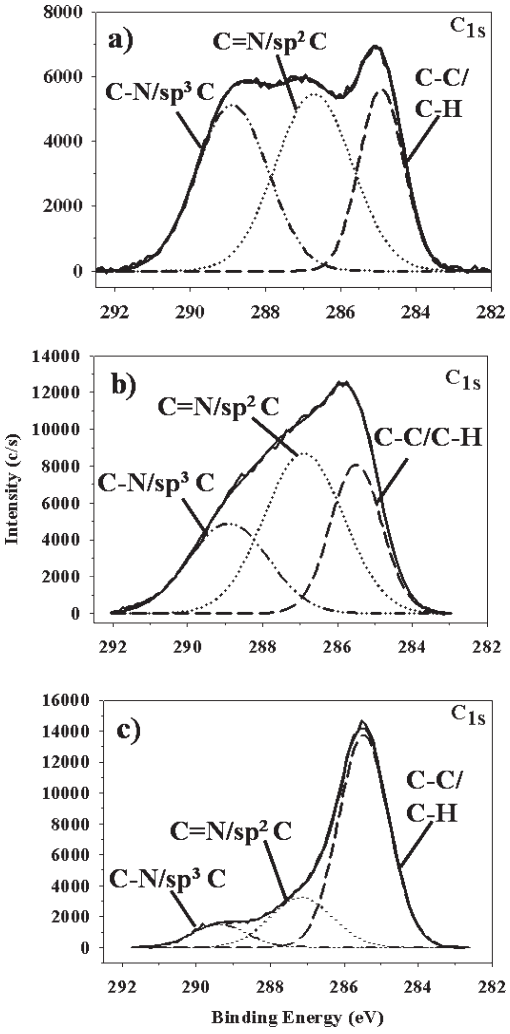

Figure 9. High-resolution C_{1s} XPS spectra for films deposited in (a) 100% BrCN; (b) 100% CH_3CN; and (c) a 50:50 $BrCN/CH_4$ plasma. The spectra are for aged samples (2−9 months) and contain three binding environments: C−C/C-H (long dash), C═N, sp^2 carbon (dotted line), and C−N, sp^3 carbon (dash-dot-dot). Plasma conditions: 100 mTorr and 50 W; BrCN and CH_3CN were run for 40 min and the $BrCN/CH_4$ mixture was run for 20 min.

An alternative hypothesis to explain the delamination behavior of our films focuses on the influence of ion bombardment during deposition. The densification of CVD films subjected to ion bombardment has been studied extensively,[29−31] and it is possible that the porosity of films deposited in BrCN discharges arises, at least in part, as a result of milder ion bombardment conditions relative to CH_3CN plasmas. The possibility of milder ion bombardment conditions in BrCN plasmas may be justified based on the presence of electronegative Br. This is illustrated by the work of Ito and co-workers, who reported dramatic decreases in electron density upon the addition of BrCN to Ar discharges.[32] Thus, if atomic Br scavenges free electrons, the ensuing decrease in electron density could be accompanied by decreases in the positive ion density and/or sheath potential, leading to a lower energy flux at the surface. Although plasma characteristics in electronegative plasmas are quite complex[33−38] and the model used here probably represents an oversimplification, it provides a means of exploring the effects of gas phase Br-content on a very basic level. Notably, deposition of a-CN_x in the presence of halogens has also been investigated by Ricci et al.[15] They studied deposition in CH_4/N_2 discharges to which small amounts ($\leq$5% of the total flow rate) of Cl_2 were added to scavenge hydrogen. Although they report changes in the physical properties and composition of the deposited films, no explanation for how Cl_2 addition causes these changes is provided.

To explore the hypothesis that Br-content is responsible for the delamination of our films, mixtures of gases were used according to a simple model that allows for variation of the effective Br-content in the gas phase. Specifically, the precursors CH_3CN, BrCN, and CH_4 were each considered in terms of the number of equivalents of Br, CH_x, and CN they contribute to the discharge. A list of the different precursor mixtures used in this study, Table 2, shows the CH_x/CN ratio is the same for each mixture, whereas the relative amount of Br varies. XPS spectra (not shown) reveal that films deposited in 1:1:1 and 14:43:43 $CH_3CN/BrCN/CH_4$ mixtures resemble those deposited in the 50/50 $BrCN/CH_4$ plasma, Figure 9c, whereas those deposited in the 3:1:1 $CH_3CN/BrCN/CH_4$ gas mixture resemble those deposited in 100% CH_3CN plasmas, Figure 9b.

Films deposited in each mixture were also characterized with VASE to extract information about the film thickness and optical properties. The growth rate data in Table 2 were calculated based on the film thicknesses and deposition times. A significant decrease in growth rate is observed as the relative equivalents of Br increase from 0 to 0.5; beyond this point, the growth rate is essentially unchanged within experimental error. This suggests that the mere presence of Br in the discharge is enough to alter the deposition behavior significantly. In addition, optical band gaps of these films were characterized in terms of the Tauc gap, E_{Tauc}, as extracted from the VASE data. The resulting data, Table 2, suggest that E_{Tauc} is highest for the three-component mixtures, which have similar E_{Tauc} values. On the basis of published studies of the optical properties of a-C:N_x,[39−46] it is possible that the trend in E_{Tauc} is related to changes in the N-content and microstructure of the material. However, additional data are needed in order to establish this trend more conclusively.

As noted above, deposition in 100% BrCN plasmas over longer times leads to immediate delamination upon removal from the reactor, and one objective of the film thickness measurements, Table 2, was to gain perspective on how growth rate varies with Br-content. The data show that films deposited in 100% CH_3CN, which never delaminate, are actually the thickest films in the series. It is evident, therefore, that delamination of the films deposited in 100% BrCN is not simply a consequence of greater film thickness; thus, we have attempted to characterize the effect of Br-content on delamination more directly. Specifically, the behavior of thick films (thickness >500 nm) was compared for three gas mixtures selected from Table 2: 100% CH_3CN, 100% BrCN, and an intermediate mixture yielding CH_x:CN:Br = 2:2:1 (the 33:33:33 $CH_3CN/BrCN/CH_4$ mixture). As discussed above, films deposited in 100% CH_3CN never delaminate, whereas films deposited in 100% BrCN consistently delaminate (for sufficient film thickness) upon exposure to atmosphere. Figure 10 shows an optical micrograph for the intermediate case; as can be seen from the image, the film has not delaminated, and this holds true even when the film is placed on a watchglass in a closed jar containing a moist sponge. This is a promising result in that it suggests that films with thicknesses on the order of several hundred nm can be deposited in the presence of Br without subsequent film delamination.

Table 2. a-CN_x Film Properties and Delamination Behavior

partial pressure (mTorr)						
CH_3CN	BrCN	CH_4	CH_x:CN:Br[b]	growth rate (nm/min)	Tauc gap, E_{Tauc} (eV)	delami-nation[a]
100			2:2:0	31 ± 4	1.5 ± 0.4	N
60	20	20	2:2:0.5	15 ± 2	2.7 ± 0.2	
33	33	33	2:2:1	13 ± 1	2.9 ± 0.2	N
14	43	43	2:2:1.5	9 ± 2	2.5 ± 0.1	
	50	50	2:2:2	13 ± 2	1.2 ± 0.2	Y

[a] Presence of delamination was empirically determined from CN_x films deposited for 40 min in 100 mTorr, 50 W plasmas of the specified compositions. [b] These ratios are based on the partial pressures of the gas-phase precursors, and are not intended to imply resulting film compositions.

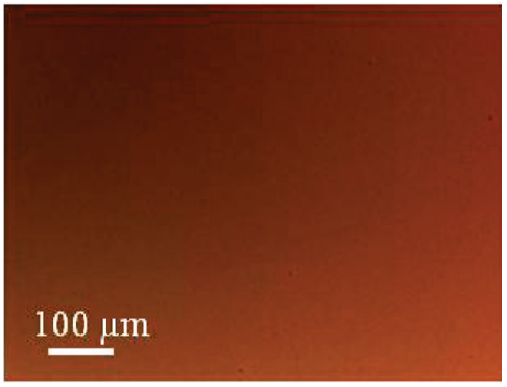

Figure 10. Phase contrast microscope image of a film deposited for 40 min in a 33:33:33 $CH_3CN/BrCN/CH_4$. The total gas pressure = 100 mTorr and rf power = 50 W.

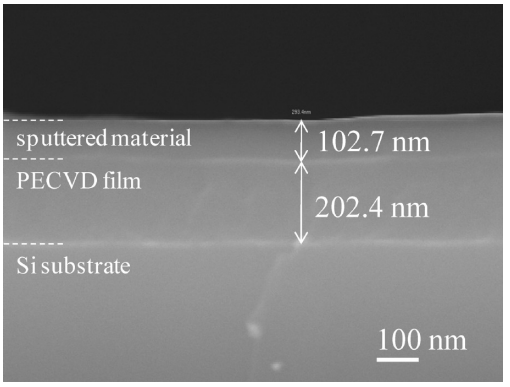

Figure 11. Cross-sectional SEM image of CN_x film deposited on Si in a 100% BrCN plasma (100 mTorr, 50 W) for 20 min and subsequently treated with a 100% N_2 plasma (100 mTorr, 50 W) for 10 min (magnification of 100 000×).

Given the aforementioned complexities associated with introducing an electronegative species such as Br into a plasma discharge, we also examined the effects of ion bombardment on a more fundamental level. Specifically, films deposited in a 100% BrCN plasma were subjected to a 10 min postdeposition treatment in a 100% N_2 plasma. For these experiments, the substrates were situated in the rf coil region to promote ion bombardment of the film. The thickness and composition were characterized using VASE and XPS, respectively, and the results were compared to control data for films deposited in a 100% BrCN plasma without postdeposition treatment. The choice of N_2 as a feed gas was made in the interest of minimizing N loss from the films, which might result from the use of a heavier bombarding species such as Ar.

Generally speaking, mild ion bombardment causes densification of plasma polymers, giving way to sputtering as the ion bombardment conditions becomes more severe.[31,47,48] In our studies, postdeposition N_2 plasma treatment at an rf power of 100 W caused the visible fringence patterns of the as-deposited films to diminish and eventually disappear. Subsequent analysis by XPS confirmed that the film had been sputtered away, leaving behind a surface composed primarily of SiO_2 with trace amounts of C, N, and Br. Based on these results, postdeposition treatment at 50 W was expected to yield a film thinner than the original but with a denser top layer due to ion bombardment. VASE data for the original film (no N_2 plasma) yielded a film thickness of 218 ± 14 nm. Postdeposition treatment in a 50 W N_2 plasma actually caused the film thickness, h, to increase by ~100 nm (h = 323 ± 37 nm). This was confirmed by cross-sectional SEM, Figure 11, and suggests that the 50 W postdeposition treatment favors sputtering and/or chemical etching[49] of material from the reactor walls and redeposition on the original film. Demarcations between different layers are visible in Figure 11, giving thicknesses within experimental error of the VASE data. Notably, XPS data show an increase in the N/C ratio following postdeposition treatment (from 0.8 ± 0.2 to 1.0 ± 0.1), suggesting that additional N incorporation occurs during redeposition and/or upon exposure to atmosphere.

As noted above and as can be seen in the optical micrographs of delaminated films, the a-CN_x films we deposit appear to undergo delamination via a "buckling-driven" mechanism.[25] This type of delamination can present as a circular pattern appearing to have originated from a blister that forms when the compressive stress forces the film to buckle away from the underlying substrate.[4,25] The blister formation is seen as a driving force on the crack interface, resulting in additional advancement of the film delamination. Studies of buckling-driven debonding have demonstrated that both circular and sinusoidal ("telephone cord") patterns can be understood as originating from an increase in compressive stress caused by water molecules diffusing through the film to the film−substrate interface.[21,23,50] The critical stress required for buckling to occur, σ_c, can be calculated using eq 3

$$\sigma_c = \frac{\pi^2 E}{12(1-\upsilon^2)}\left(\frac{h}{b}\right)^2 \quad (3)$$

Where E = the elastic modulus of the film, υ = Poisson's ratio, h = film thickness, and b = the half blister width. Although we have

not directly measured E and ν for our films, Peponas et al. have done so for a-C:N_x films that are similar in composition to those deposited here.[21,23,50] Thus, if we assume their values for our films, E = 22.5 GPa and ν = 0.3, we can calculate an approximate value for σ_c. Using the film thickness/deposition rate data presented above and in Table 2 and estimating b from the micrographs shown in Figure 1b and 6, we find $\sigma_c = 1.2 \pm 0.2$ MPa for films deposited from 100% BrCN plasmas and $\sigma_c = 7.8 \pm 1.6$ MPa for films deposited from 50:50 BrCN/CH_4 plasmas. These values are similar to those obtained by Peponas et al. for a-CN_x films deposited via magnetron sputtering, who found σ_c ranged from ~1 MPa up to ~30 MPa, depending on the thickness of the deposited film.[50] Moreover, our estimated values support the observation that films deposited in 100% BrCN plasmas delaminate more rapidly than those deposited in other gas mixtures as a lower σ_c indicates a lower barrier to delamination. Unfortunately, the uncertainty associated with measuring the "curvature" of our films from the optical micrographs, as posited by Peponas et al., was sufficiently high that we are not confident in our ability to estimate the intrinsic stress in the films deposited in BrCN plasmas. Nevertheless, the differences we observe in the delamination behavior of our films are likely the result of a combination of an increase in compressive stress as a result of moisture diffusion and an increase in intrinsic stress resulting from changes in nitrogen content in the films.

SUMMARY

The delamination of a-CN_x films deposited in plasma discharges containing BrCN was explored and is largely attributed to H_2O diffusion to the film−substrate interface. Attempts to understand this behavior therefore focused on two approaches to controllably altering the film microstructure. The first involved the introduction of hydrocarbons (in the form of CH_4) into the discharge, with the intention of promoting cross-linking (and thereby reducing porosity). These studies, however, suggested this approach did not prevent delamination of the film from the underlying substrate. The second approach investigated the effects of ion bombardment on deposition through variation of the effective Br-content in the discharge and postdeposition treatment of a-CN_x films in a 100% N_2 plasma. This latter study did not cause densification of the films, but resulted in sputtering and redeposition of materials from the reactor walls. In contrast, the experiments in which gas phase Br-content was varied revealed reproducible changes in the growth rate and optical properties of the deposited material, suggesting Br alters the deposition conditions in such a way as to promote film delamination. We also find, however, that a-CN_x film adhesion can be maintained when the effects of Br addition are attenuated (e.g., by additional hydrocarbon content in the plasma) even under humid conditions.

AUTHOR INFORMATION

Corresponding Author

*E-mail: ellen.fisher@colostate.edu.

ACKNOWLEDGMENT

This work was supported by the National Science Foundation (NSF-0911248). We thank Dr. Carmen Menoni for use of the phase contrast microscope and Dr. Sandeep Kohli for assistance with the VASE models.

REFERENCES

(1) Mishnaevsky, L. L.; Gross, D., Jr. *Int. Appl. Mech.* **2004**, *40*, 140–155.
(2) Shugurov, A. R.; Panin, A. V. *Phys. Mesomech.* **2010**, *13*, 79–87.
(3) Kim, T.-S.; Dauskardt, R. H. *IEEE Trans. Device Mater. Reliab.* **2009**, *9*, 509–515.
(4) Moller, J.; Reiche, D.; Bobeth, M.; Pompe, W. *Surf. Coatings Technol.* **2002**, *150*, 8–14.
(5) Lejeune, M.; Benlahsen, M.; Lemoine, P. *Solid-State Commun.* **2005**, *135*, 434–439.
(6) Liu, D.; Fisher, E. R. *J. Vac. Sci. Technol., A* **2007**, *25*, 368–377.
(7) Stillahn, J. M.; Fisher, E. R. *J. Phys. Chem. C* **2009**, *113*, 1963–1971.
(8) Stillahn, J. M.; Fisher, E. R. *J. Phys. Chem. A* **2010**, *114*, 5287–5294.
(9) Ito, H.; Ozaki, Y.; Suzuki, K.; Kondow, T.; Kuchitsu, K. *J. Chem. Phys.* **1992**, *96*, 4195–4204.
(10) Schaefer, H. F., III; Heil, T. G. *J. Chem. Phys.* **1971**, *54*, 2573–2580.
(11) Ito, H.; Ito, N.; Takahashi, T.; Takamatsu, H.; Tanaka, D.; Saitoh, H. *Jpn. J. Appl. Phys., Part I* **2000**, *39*, 1371–1377.
(12) Mendez, J. M.; Gaona-Couto, A.; Muhl, S.; Jimenez-Sanoval, S. *J. Phys.: Condens. Matter* **1999**, *11*, 5225–5235.
(13) Hellgren, N.; Johansson, M. P.; Hjorvarsson, B.; Broitman, E.; Ostblom, M.; Liedberg, B.; Hultman, L.; Sundgren, J.-E. *J. Vac. Sci. Technol. A* **2000**, *18*, 2349–2358.
(14) Hammer, P.; Victoria, N. M.; Alvarez, F. *J. Vac. Sci. Technol., A* **1998**, *16*, 2941–2949.
(15) Ricci, M.; Trinquecoste, M.; Auguste, F.; Canet, R.; Delhaes, P.; Guimon, C.; Pfister-Guillouzo, G.; Nvesten, B.; Issi, J. P. *J. Mater. Res.* **1993**, *8*, 480–488.
(16) Saitoh, H.; Takamatsu, H.; Tanaka, D.; Ito, N.; Ohshio, S.; Ito, H. *Jpn. J. Appl. Phys., Part I* **2000**, *39*, 1258–1263.
(17) Bogart, K. H. A.; Dalleska, N. F.; Bogart, G. R.; Fisher, E. R. *J. Vac. Sci. Technol., A* **1995**, *13*, 476–480.
(18) Truica-Marasescu, F.; Jedrzejowski, P.; Wertheimer, M. R. *Plasma Process. Polym.* **2004**, *1*, 153–163.
(19) Jellison, G. E.; Modine, F. A. *Phys. Rev. B* **1983**, *27*, 7466–7472.
(20) Jellison, G. E. *Opt. Mater.* **1992**, *1*, 41–47.
(21) Peponas, S.; Guedda, M.; Benlahsen, M. *Solid State Commun.* **2008**, *146*, 78–82.
(22) Peponas, S.; Benlahsen, M.; Guedda, M. *J. Appl. Phys.* **2009**, *106*, 013525.
(23) Peponas, S.; Guedda, M.; Benlahsen, M. *Appl. Surf. Sci.* **2009**, *255*, 8706–8709.
(24) Papirer, E.; Lacroix, R.; Donnet, J.-B.; Nanse, G.; Fioux, P. *Carbon* **1994**, *32*, 1342–1358.
(25) Hutchinson, J. W.; Thouless, M. D.; Liniger, E. G. *Acta Metall. Mater.* **1992**, *40*, 295–308.
(26) Lin, Y.; Tsui, T. Y.; Vlassak, J. J. *J. Electrochem. Soc.* **2010**, *157*, G53–G56.
(27) von Keudell, A.; Schwarz-Selinger, T.; Jacob, W. *J. Appl. Phys.* **2001**, *89*, 2979.
(28) Kim, K. B.; Kim, S. H. *J. Vac. Sci. Technol., A* **2000**, *18*, 900–906.
(29) Amassian, A.; Vernhes, R.; Klemberg-Sapieha, J. E.; Desjardins, P.; Martinu, L. *Thin Solid Films* **2004**, *469−470*, 47–53.
(30) Vlcek, J.; Rusnak, K.; Hajek, V.; Martinu, L. *J. Appl. Phys.* **1999**, *86*, 3647–3654.
(31) Bakai, A. S.; Zhukov, A. I.; Sleptsov, S. N. *J. Phys. D: Condens. Matter* **1999**, *11*, 5681–5689.
(32) Ito, H.; Miki, H.; Namiki, K. C.; Ito, N.; Saitoh, H. *J. Vac. Sci. Technol., A* **2004**, *22*, 487.
(33) Marakhatanov, A. M.; Tuszewski, M.; Lieberman, M. A.; Lichtenberg, A. J.; Chabert, P. *J. Vac. Sci. Technol., A* **2003**, *21*, 1849–1864.

(34) Franz, G. *J. Vac. Sci. Technol., A* **2005**, *23*, 369–387.
(35) Li, M.; Vyvoda, M. A.; Dew, S. K.; Brett, M. J. *IEEE Trans. Plasma Sci.* **2000**, *28*, 248–252.
(36) Sheridan, T. E.; Chabert, P.; Boswell, R. W. *Plasma Sources Sci. Technol.* **1999**, *8*, 457–462.
(37) Chung, T. H. *Phys. Plasmas* **2009**, *16*, 063503.
(38) Kouznetsov, I. G.; Lichtenberg, A. J.; Lieberman, M. A. *J. Appl. Phys.* **1999**, *86*, 4142–4153.
(39) Silva, S. R. P.; Robertson, J.; Amaratunga, G. A. J.; Rafferty, B.; Brown, L. M.; Schwan, J.; Fanceschini, D. F.; Mariotto, G. *J. Appl. Phys.* **1997**, *81*, 2626–2634.
(40) Canillas, A.; Polo, M. C.; Andujar, J. L.; Sancho, J.; Bosch, S.; Robertson, J.; Milne, W. I. *Diamond Relat. Mater.* **2001**, *10*, 1132–1136.
(41) Godet, C.; Adamopoulos, G.; Kumar, S.; Katsuno, T. *Thin Solid Films* **2005**, *482*, 24–33.
(42) Hayashi, Y.; Yu, G.; Rahman, M. M.; Krishna, K. M.; Soga, T.; Jimbo, T.; Umeno, M. *Appl. Phys. Lett.* **2001**, *78*, 3962.
(43) Jelinek, M.; Kulisch, W.; Delplancke-Ogletree, M. P.; Lancok, J.; Jastrabik, L.; Chvostova, D.; Popov, C.; Bulir, J. *Appl. Phys. A: Mater. Sci. Process.* **2001**, *73*, 167–170.
(44) Rodil, S. E.; Muhl, S.; Maca, S.; Ferrari, A. C. *Thin Solid Films* **2003**, *433*, 119–125.
(45) Tsubouchi, N.; Enders, B.; Chayahara, A.; Kinomura, A.; Heck, C.; Horino, Y. *J. Vac. Sci. Technol. A* **1999**, *17*, 2384–2388.
(46) Wei, J.; Hing, P. *J. Appl. Phys.* **2002**, *91*, 2812–2817.
(47) Hess, D. W.; Graves, D. B., . In *Chemical Vapor Deposition: Principles and Applications*; Hitchman, M. L., Jensen, K. F., Eds. Academic Press: San Diego, CA, 1993; pp 385−435.
(48) Nastasi, M.; Misra, A.; Mayer, J. W., . In *Materials Processing Handbook*, Groza, J. R., Ed.; CRC Press LLC: Boca Raton, FL, 2007; pp 1−24.
(49) Hammer, P.; Gissler, W. *Diamond Relat. Mater.* **2006**, *5*, 1152–1158.
(50) Peponas, S.; Benlahsen, M.; Guedda, M. *J. Appl. Phys.* **2009**, 106.